# Azimuthally anisotropic effective parameters from full-azimuth reflection angle gathers

*Liron Korkidi\*, Raz Litvak, Cindy Ayache, Ronit Levy and Zvi Koren, Emerson*

## Summary

We present an efficient and stable procedure for estimating second- and fourth-order azimuthally-dependent effective parameters from full-azimuth residual moveouts. The residual moveouts are automatically picked at depth image points along full-azimuth angle domain reflection angle gathers. It is assumed that the azimuthally varying residual moveouts are due to fracture systems within compacted sand/shale sediment layers which were not accounted for in the seismic migration. The extracted (up to eight) effective parameters can then be used to obtain local (layer) effective parameters, characterizing the intensity and orientation of the fracture systems at each layer. Finally, the local effective parameters can be inverted to obtain interval anisotropic (e.g., orthorhombic) model parameters to be used in orthorhombic seismic migration.

## Introduction

We consider a layered model, where some of the target layers contain near vertically aligned fracture systems, with different orientations at each layer. A background azimuthally-isotropic (e.g., ISO or VTI) velocity model is first derived and used for migrating the recorded seismic data into depth domain full-azimuth reflection angle gathers (Koren et al., 2007). Since the fracture parameters were not included in the migration velocity field, periodic azimuthally varying residual moveouts (RMOs) are clearly seen at major reflectors along the migrated gathers (Figure 1). Automatic event picking based on a stable Poisson tracking algorithm (Bartana et al., 2011) is used to detect the RMOs. Using the background migration velocity and the automatically picked RMOs, the proposed workflow includes three main stages. First, following the theory presented in papers by Koren and Ravve (2014, 2017), we estimate for each reflection point a set of (up to eight) global effective parameters using an explicit fourth-order approximation formula which best fits the azimuthally-varying picked RMOs. The second stage includes a constrained generalized Dix-type approach for converting the global effective parameters into local (layer) parameters. These local effective parameters provide reliable information about the existence (or absence) of aligned fracture systems within the layers, their intensity (tectonic stress) and their orientation. In many cases, this intermediate information is already very valuable for production engineers, for improving well planning and enhancing O&G recovery. The last stage involves conversion of the local effective parameters into interval orthorhombic velocity parameters (Koren et al., 2013), which can then be used as input for an orthorhombic depth migration. The goal of the proposed inversion is to generate a reliable orthorhombic layered model that yields flatter full-azimuth reflection angle gathers, and to improve the quality and accuracy of the depth image. In this Abstract, we concentrate on the first stage of the workflow, i.e. extracting the azimuthally-dependent global effective parameters from the full-azimuth reflection angle gathers. We demonstrate the strength of our method by applying it to both synthetic and field datasets.
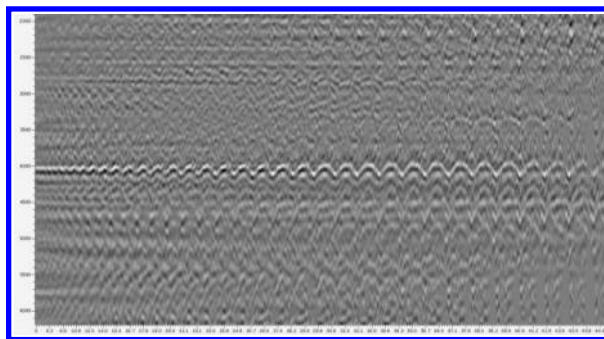


Figure 1: An example of a full-azimuth reflection angle gather from the Barnett Shale. The reflection angle increases along the horizontal axis, while the azimuth varies periodically (spiral). The oscillations in the azimuthally varying moveout suggest that this is a fractued area.

## Fourth-order residual moveout (RMO) approximation

The asymptotic nonhyperbolic traveltime approximation, first suggested by Tsvankin and Thomsen (1994) for azimuthally isotropic layered media, has also been widely used for azimuthally anisotropic models (Xu et al., 2005; Vasconcelos et al., 2006),

$$t^2\left(t_{\mathrm{o}},\psi_{\mathrm{off}},h\right)=t_{\mathrm{o}}^2+\frac{h^2}{V_2^2}\left(1-\frac{\left(V_4^4-V_2^4\right)h^2}{4V_2^6 t_{\mathrm{o}}^2+\left(3V_2^4+V_4^4\right)h^2}\right),\ (1)$$

where $t_{\mathrm{o}}$ is the vertical time, $h$ is the offset, $\psi_{\mathrm{off}}$ is the offset domain azimuth, and $V_2\left(\psi_{\mathrm{off}}\right)$ and $V_4\left(\psi_{\mathrm{off}}\right)$ are the second- and fourth-order azimuthally-dependent normal moveout (NMO) velocities. In many cases, a quartic term $\eta=\left(V_4^4-V_2^4\right)/8V_2^4$ is used instead of $V_4$.

In this work, we directly analyze residual moveouts (RMOs) measured along depth migrated gathers. The corresponding residual moveout formula can be obtained by calculating the full differential of Eq. 1 and setting to zero the total traveltime changes. Moreover, since the migrated gathers are performed in the angle (slowness) domain, the offsets should be explicit functions of angles, and the second- and fourth-

order NMO velocities should be given as functions of the slowness-azimuths $\psi = \psi_{\text{slw}}$, $V_2(\psi)$ and $V_4(\psi)$ (Koren and Ravve, 2017). The corresponding residual moveout formula is given by

$$\frac{\Delta t_o(t_o,\psi,\theta)}{t_o} = \left(\frac{\partial t^2/\partial^2 V_2}{\partial t^2/\partial^2 t_o}\right)\frac{V_2}{t_o}\alpha_2 + \left(\frac{\partial t^2/\partial^2 V_4}{\partial t^2/\partial^2 t_o}\right)\frac{V_4}{t_o}\alpha_4, \quad (2)$$

where $\alpha_2(\psi)$ and $\alpha_4(\psi)$ are the second- and fourth-order relative residual velocities,

$$\alpha_2(\psi) = \frac{V_2^{up}(\psi) - V_2^{bg}}{V_2^{bg}}; \quad \alpha_4(\psi) = \frac{V_4^{up}(\psi) - V_4^{bg}}{V_4^{bg}}, \quad (3)$$

where the superscripts *up* and *bg* refer to updated and background, respectively. Eq. 2 can be separated into azimuthally-dependent and azimuthally-independent functions

$$\frac{\Delta t_o(t_o,\psi,\theta)}{t_o} = -F_2(\theta)\alpha_2(\psi) - F_4(\theta)\alpha_4(\psi). \quad (4)$$

The azimuthally-independent part is only a function of the background azimuthally-isotropic velocities, given by

$$F_2(\theta) = -\frac{8h^2V_2^2}{\Delta t_o}\left(3h^2V_2^4 + 2t_o^2V_2^6 - h^2V_4^4\right)$$

$$F_4(\theta) = -\frac{16h^4V_4^4}{Dt_o}\left(h^2 + t_o^2V_2^2 - V_4^4\right), \quad (5)$$

where $D = \left[h^2\left(3V_4^4 + V_4^4\right) + 4t_o^2V_2^6\right]^2$, $V_2 = V_2^{bg}$ and $V_4 = V_4^{bg}$.

**Obtaining the second- and fourth-order effective velocity parameters**

The input for our procedure is azimuthally-varying RMO curves extracted from migrated gathers. The analysis is done in two stages:

- Discretizing the auto-picked RMO data into azimuth sectors between 0 to 180 degrees (every one or two degrees). For each azimuth sector, converting the RMOs to second- and fourth-order relative residual velocities (Eq. 2) and forming two arrays,

$$V_2^{up}(\psi_i) = V_2^{bg}\left(1 + \alpha_2(\psi_i)\right),$$

$$V_4^{up}(\psi_i) = V_4^{bg}\left(1 + \alpha_4(\psi_i)\right). \quad (6)$$

- Applying a Fourier transform to $V_2^{up}(\psi_i)$ and $V_4^{up}(\psi_i)$ and extracting eight (three second-order and five fourth-order) effective parameters $\left\{V_{2H}, V_{2L}, \psi_{2L}, \bar{V}_4, V_{4H}, V_{4L}, \psi_{42}, \psi_{44}\right\}$.

This is an extension to the method proposed by Koren and Ravve (2014) for second-order parameters only.

The second- and fourth-order NMO velocities are given by

$$V_2^2(\psi) = V_{2H}^2\sin^2(\psi - \psi_{2L}) + V_{2L}^2\cos^2(\psi - \psi_{2L}),$$

$$V_4^4(\psi) = \bar{V}_4^4 + \frac{V_{4H}^4 - V_{4L}^4}{2}\frac{\cos[2(\psi - \psi_{42})]}{\cos(2(\psi_{44} - \psi_{2L}))} + \frac{V_{4H}^4 - 2\bar{V}_4^4 + V_{4L}^4}{2}\frac{\cos[4(\psi - \psi_{44})]}{\cos(4(\psi_{42} - \psi_{2L}))}. \quad (7)$$

First, we apply the method on a synthetic model with three orthorhombic layers, each oriented in a different direction (Table 1).

| $\Delta z$ [km] | $v$ [km/s] | $\delta_1$ | $\delta_2$ | $\epsilon_1$ | $\epsilon_2$ | $\phi$ [deg] |
|---|---|---|---|---|---|---|
| 1 | 3 | 0.07 | -0.05 | 0.1 | 0.2 | 20 |
| 1 | 3 | 0.15 | -0.2 | 0.15 | 0.1 | 55 |
| 1 | 3 | 0.1 | -0.0075 | 0.2 | 0.25 | 110 |

Table 1: Synthetic model with three orthorhombic layers. Each layer is described by different Tsvankin parameters.

The azimuthally-varying moveout curves picked on the spiral reflection angle gather are shown in Figure 2 and are the input for the proposed method. The inverted $V_2^{up}(\psi_i)$ and $V_4^{up}(\psi_i)$ are shown in Figure 3.
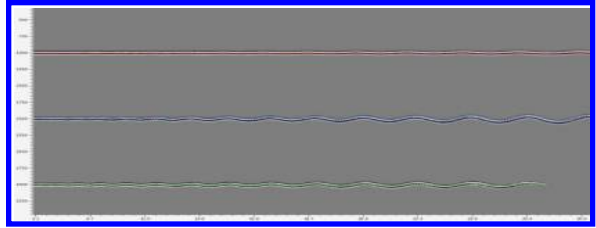


Figure 2: The VTI migrated reflection angle gathers for a 3-layer synthetic model. The oscillations of the (spiral) azimuthally-dependent moveout are in very good agreement with the Poisson auto-picked residual moveout curves---hor1 (red), hor2 (blue), hor3 (green).
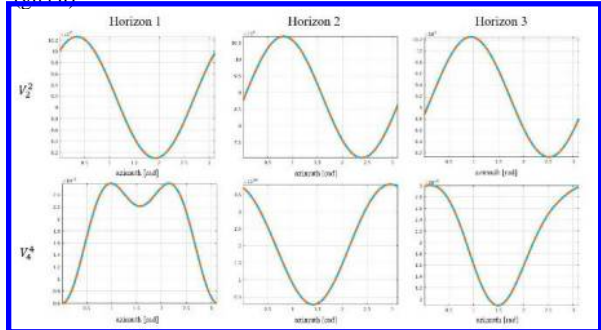


Figure 3: The second-order (top) and fourth-order (bottom) velocities as a function of the azimuth. We show the results for all 3 horizons, where the dashed orange curve is the result of the least square inversion and the blue curve is the forward analytic calculation.

# Azimuthally anisotropic effective parameters from full-azimuth reflection angle gathers

Figure 4 shows the Fourier components of the second- and fourth-order parameters and their relation to our proposed effective velocity parameters.
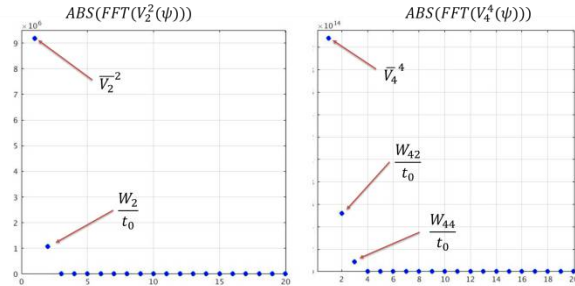


Figure 4: The Fourier transform of the $2^{nd}$ NMO velocity (right) and $4^{th}$ NMO velocity (left) of the first horizon in the synthetic model. From the marked components, we calculate the 8 effective parameters of the orthorhombic model.

The Fourier transform of the second order NMO velocity can be described using two components. The DC component describes the azimuthally-independent part $\bar{V}_2$ while the first harmonic is a complex number with magnitude $e_2 = W_2 / t_o$. Three effective parameters can be calculated directly from these components,

$$V_{2L}^2 = \bar{V}_2^2 \left(1 - e_2\right), \; V_{2H}^2 = \bar{V}_2^2 \left(1 + e_2\right),$$

$$\psi_{2L} = \tan^{-1}\left(e_{2y} / e_{2x}\right). \tag{8}$$

The Fourier transform of the fourth-order NMO velocity can be described by three components. The DC component describes the azimuthally-independent part $\bar{V}_4$ and the two harmonics are complex numbers $W_{42}$ and $W_{44}$. From these five components we calculate the additional five effective parameters $\bar{V}_4$, the low and high fourth-order velocities and two additional azimuths,

$$V_{4L}^4 = 2\frac{\bar{V}_4^4}{t_o} - 2\frac{W_{2x}W_{42x} + W_{2y}W_{42y}}{W_2 t_o} + \frac{W_{44x}\left(W_{2x}^2 - W_{2y}^2\right) + 2W_{2x}W_{2y}W_{44y}}{W_2 t_o}$$

$$V_{4H}^4 = 2\frac{\bar{V}_4^4}{t_o} + 2\frac{W_{2x}W_{42x} + W_{2y}W_{42y}}{W_2 t_o} + \frac{W_{44x}\left(W_{2x}^2 - W_{2y}^2\right) + 2W_{2x}W_{2y}W_{44y}}{W_2 t_o}$$

$$\psi_{42} = 0.5 \cdot \tan^{-1}\left(W_{42y} / W_{42x}\right)$$

$$\psi_{42} = 0.25 \cdot \tan^{-1}\left(W_{44y} / W_{44x}\right). \tag{9}$$

By using this extraction method on the input synthetic azimuthally-dependent moveouts, we obtain very good results compared to the analytically calculated effective parameters (Table 2).

| $V_{2H}$ | $V_{2L}$ | $\psi_{2L}$ | $\bar{V}_4$ | $V_{4H}$ | $V_{4L}$ | $\psi_{42}$ | $\psi_{44}$ |
|---|---|---|---|---|---|---|---|
| 3.2 | 2.84 | 20.01 | 3.72 | 3.95 | 3.31 | 0 | 0 |
| 3.26 | 2.84 | 20.9 | 3.72 | 3.94 | 3.41 | 0.27 | 1.68 |
| 3.27 | 2.65 | 47.02 | 3.8 | 4.1 | 3.47 | 40.6 | 1.25 |
| 3.34 | 2.67 | 48.6 | 3.8 | 3.67 | 3.55 | 21.8 | 0.37 |
| 3.2 | 2.85 | 54.12 | 3.8 | 3.98 | 3.64 | 40.8 | 6.11 |
| 3.2 | 2.83 | 54.98 | 3.8 | 3.71 | 3.45 | 37.76 | 5.45 |

Table 2: Comparison of the eight effective parameters for all three layers of the synthetic model. The moveout calculated directly from the interval parameters is on top (blue) and the effective parameters as extracted from the azimuthally-dependent residual moveout are at the bottom (orange).

The eight global effective parameters are then converted to local effective parameters for each layer using generalized Dix-type inversion, and then to interval parameters. The interval parameters are used in the ray tracing of the full orthorhombic migration, resulting in fairly flattened gathers for all three layers (Figure 5).
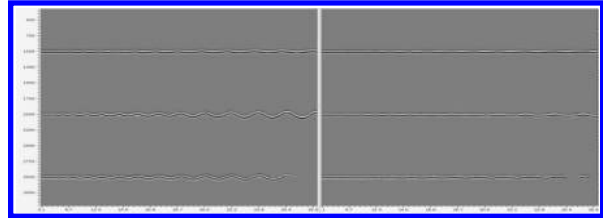


Figure 5: The full-azimuth reflection angle gathers after VTI migration (left) and after full orthorhombic migration (right). All three orthorhombic layers were flattened in the orthorhombic migration.

**Reliability Factor**

We define a reliability factor to assess the accuracy of the calculated effective parameters. The reliability factor is a multiplication of three terms

$$R = R_1 \cdot R_2 \cdot R_3. \tag{10}$$

The first is a semblance factor which accounts for the quality of the tracking procedure. Areas with poor data have low reliability value, while areas with a clear reflection event have a value of about one.

The second term is a measure of the strength of the azimuthal dependency of the moveout, and is given by the difference between the second-order NMO velocities in the direction of the fractures and perpendicular to them,

$$R_2 = \frac{\Delta\alpha}{MAX\left(\Delta\alpha\right)}; \quad \Delta\alpha = \frac{V_{2H} - V_{2L}}{V_2^{bg}}.$$

The third term measures the accuracy of the procedure defined in this abstract by comparing the input residual moveout which was picked on the full-azimuth reflection

# Azimuthally anisotropic effective parameters from full-azimuth reflection angle gathers

gather, and the residual moveout calculated analytically from the extracted effective parameters,

$$R_3 = \frac{Cov\left(\Delta t^{track}, \Delta t^{calc}\right)}{Var\left(\Delta t^{track}\right)Var\left(\Delta t^{calc}\right)} \ .$$

## Field example

Full-azimuth reflection angle gathers were generated using VTI migration for the Barnett Shale dataset. Figure 6 shows an example of the resulting migrated gathers as a function of the reflection angle and azimuth. The layer of interest is marked by a dashed blue line (at around 4200ft), where a clear azimuthally-varying moveout is observed.
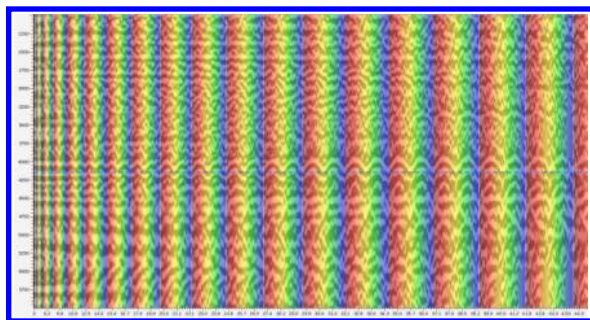


Figure 6: An example of a full-azimuth reflection angle gather from the Barnett Shale overlayed by the azimuths to emphasize the azimuthal periodicity of the RMO oscillations.

This azimuthally-varying residual moveout was automatically picked by the 2D Poisson tracking algorithm. The resulting curve is shown in Figure 7 (green curve). On the picked RMO curve, we ran the workflow described above to obtain the eight global effective parameters. The eight extracted effective parameters were then used to analytically calculate a residual moveout curve as given by Eq. 2. The calculated RMO curve is shown in Figure 7 (red curve), and nicely fits the picked (green) curve.
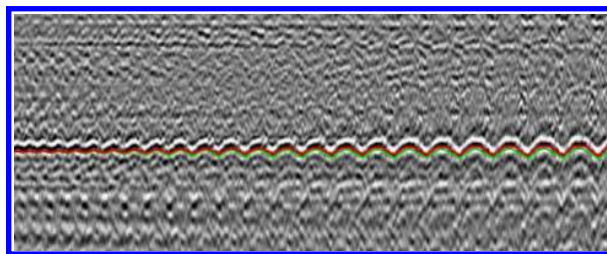


Figure 7: The green curve is the result of the auto tracking Poisson algorithm for the layer of interest. The red curve is the RMO curve which was calculated analytically from the eight extracted effective parameters.

Figures 6 and 7 display areas where the azimuthally varying signature is pronounced; however, this is not the case for all locations (e.g. inline, crossline). At some locations, the VTI migrated gathers have no azimuthal dependency. To account for this effect, we used the reliability factor given by Eq. 10. In Figure 8 we show an example of two locations, one with a high reliability factor and one with a low factor. Indeed, in areas where the moveout does not vary with azimuth, we obtain a low reliability factor.
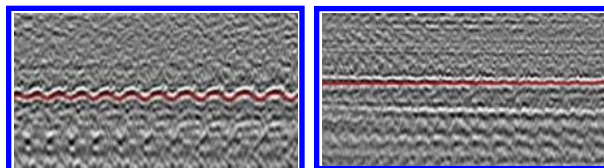


Figure 8: The azimuthally picked curves on top of the migrated gather at two different locations. In an area where the azimuthal dependency is pronounced (left), the reliability is high. In an area where the gathers are relatively flat (right), the reliability is low.

Finally, we completed the workflow using the extracted effective parameters to obtain gathers after orthorhombic migration. We first used a Dix-type inversion to calculate the local (layer) parameters, and then inverted the local parameters to the interval velocity parameters. The interval parameters were then used to run a full-azimuth orthorhombic migration, resulting in flat gathers as expected (Figure 9).
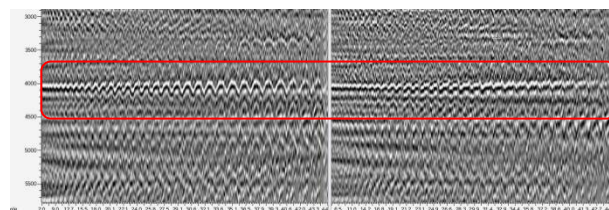


Figure 9: The full-azimuth reflection angle gathers after VTI migration (left) and after full orthorhombic migration (right). The orthorhombic layer at 4200ft is flat.

## Conclusions

We describe a new method for automatically extracting eight global effective parameters characterizing the kinematical characteristics of an orthorhombic layered medium. The success of the proposed method is due to the high quality full-azimuth reflection angle gathers that make it possible to reliably detect the corresponding RMOs. By converting the RMOs into azimuthally-varying second- and fourth-order NMO velocities, and using their periodic nature, we successfully extracted the eight effective parameters for both synthetic and field data.

# REFERENCES

Bartana, A., D. Kosloff, and Y. Hollander, 2011, Automatic picking of delays on 3D angle gathers: 80th Annual International Meeting, SEG, Expanded Abstracts, 3903–3907, https://doi.org/10.1190/1.3628020.

Koren, Z., and I. Ravve, 2014, Azimuthally dependent anisotropic velocity model update: Geophysics, **79**, no. 2, C27–C53, https://doi.org/10.1190/geo2013-0178.1.

Koren, Z., and I. Ravve, 2017, Fourth-order normal moveout velocity in elastic layered orthorhombic media—Part 2: Offset-azimuth domain: Geophysics, **82**, no. 3, C113–C132, https://doi.org/10.1190/geo2016-0222.1.

Koren, Z., I. Ravve, A. Bartana, and D. Kosloff, 2007, Local angle domain in seismic imaging: 69th Annual International Conference and Exhibition, EAGE, Extended Abstracts, https://doi.org/10.3997/2214-4609.201401932.

Koren, Z., I. Ravve, and R. Levy, 2013, Conversion of background VTI depth model and full-azimuth reflection angle moveouts into interval orthorhombic layered parameters: 75th Annual International Conference and Exhibition, EAGE, Extended Abstracts, https://doi.org/10.3997/2214-4609.20130943.

Tsvankin, I., and L. Thomsen, 1994, Nonhyperbolic reflection moveout in anisotropic media: Geophysics, **59**, 1290–1304, https://doi.org/10.1190/1.1443686.

Vasconcelos, I., and I. Tsvankin, 2006, Non-hyperbolic moveout inversion of wide-azimuth P-wave data for orthorhombic media: Geophysical Prospecting, **54**, 535–552, https://doi.org/10.1111/j.1365-2478.2006.00559.x.

Xu, X., I. Tsvankin, and A. Pech, 2005, Geometrical spreading of P-waves in horizontally layered, azimuthally anisotropic media: Geophysics, **70**, no. 5, D43–D53, https://doi.org/10.1190/1.2052467.